PERGAMON

International Journal of Multiphase Flow 28 (2002) 1311–1331

International Journal of Multiphase Flow

www.elsevier.com/locate/ijmulflow

The influence of small tube diameter on falling film and flooding phenomena

A.A. Mouza, S.V. Paras, A.J. Karabelas *

Department of Chemical Engineering, and Chemical Process Engineering Research Institute, Aristotle University of Thessaloniki, University Box 455, GR 54124 Thessaloniki, Greece

Received 7 October 2001; received in revised form 1 May 2002

Abstract

Flooding experiments have been carried out in vertical small i.d. tubes (6, 7, 8 and 9 mm), using smooth inlet and outlet conditions, with air and two liquids (water and kerosene). Experimental data on free falling film characteristics have also been obtained, in the same test sections, which aid the interpretation of flooding phenomena. These new data suggest that the tube diameter strongly affects film flow development, possibly promoting wave interaction and damping. In turn, the wavy film evolution essentially determines flooding characteristics. At small liquid Reynolds numbers ($Re_L < 300$) critical flooding velocities, U_G, follow a trend already reported in the literature, i.e. decreasing with increasing liquid rate. However, at higher Re_L the trend is reversed, i.e. increasing U_G with increasing liquid rate. This has not been reported in the literature before and may be attributed to damping of waves. At still higher Re_L, another region is evident in the flooding curves, characterized by nearly constant flooding velocity. The dominant mechanism in almost all cases is wave growth and upward dragging by the gas, initiated at the liquid exit.

Keywords: Flooding; Falling film; Vertical small diameter tube; Low Reynolds number

1. Introduction

Flooding is of importance as a limiting factor in the operation of common process equipment such as reflux condensers, wetted wall columns etc. This phenomenon results from the interaction

* Corresponding author. Tel.: +30-310-996201; fax: +30-310-996209.
E-mail address: karabaj@cperi.certh.gr (A.J. Karabelas).

0301-9322/02/$ - see front matter
PII: S0301-9322(02)00033-2

between a gas flowing upwards inside a conduit and a liquid falling counter-currently at the wall. More precisely, *incipient flooding* may be described as the condition where at least part of the liquid film flow is reversed in direction and carried above the point of liquid injection.

In recent years there is considerable interest in understanding flooding of narrow flow passages, resulting mainly from efforts to develop compact devices such as plate heat exchangers and condensers. Counter-current gas/liquid flow in *small diameter* tubes is considered an essential element of the complicated flow field of a compact reflux condenser, usually made of corrugated plates. Typical flow passages therein are characterized by equivalent diameters less than 10 mm. Usually liquid loadings in the aforementioned equipment are small to moderate, corresponding to superficial liquid Reynolds numbers $Re_L = 4\Gamma/v$ below 1000. Motivated by the above considerations this work is focused on flooding and liquid film flow through small diameter tubes (with i.d. 6 to 9 mm) for Re_L in the range 10 to 1000.

Although flooding has been studied extensively in the past few decades, there is still considerable uncertainty concerning the prevailing mechanisms as well as the most appropriate correlations for practical applications. Bankoff and Lee (1986) and Hewitt (1995) have reviewed and summarized the work done in this area, most of which is based on experiments in pipes with i.d. much larger than the sizes considered here. In general, the factors that tend to influence the onset of flooding are (e.g. Hewitt, 1995; Zapke and Kroeger, 1996) the conduit dimensions, the type of liquid and gas entry and the properties of the liquid. For a smooth liquid entry, the type of gas entry appears to play a significant role. A tapered tube-end (promoting a fairly well developed entering gas flow with reduced disturbances) is associated with greater flooding velocities than a sharp-edged end (Hewitt, 1995). As regards tube size, the general trend is an increased flooding velocity with increasing tube i.d. (e.g. Koizumi and Ueda, 1996). There is also evidence that the critical flooding velocity tends to decrease with increasing liquid viscosity (e.g. Clift et al., 1966) and decreasing surface tension (e.g. Zapke and Kroeger, 2000b).

There has been considerable debate in the past (e.g. Moalem Maron and Dukler, 1984; Hewitt, 1995) concerning the dominant mechanisms of flooding in vertical tubes. However, in recent years there appears to be an agreement (Hewitt, 1995; Jayanti et al., 1996) that flooding is brought about by two types of gross mechanisms, i.e. upward transport of waves mainly from the area close to liquid outlet, and carryover of droplets from disintegration of the falling liquid film. The former mechanism seems to dominate in relatively small diameter tubes (where the total drag exerted by the gas on waves can overcome the gravity force), whereas the latter is evident in large i.d. tubes and is associated with higher flooding velocities. It will be pointed out here that the experimental evidence that helped identify these trends, was obtained with tube diameters much larger than those considered in the present study.

Recognizing that the cause of flooding resides in the complicated interaction of gas flow with a wavy liquid film interface, some theoretical attempts have been made to model flooding (e.g. Shearer and Davidson, 1965; Centinbudaklar and Jameson, 1969) based on liquid wave growth and stability analysis. The success of such efforts has been limited at best.

In view of the aforementioned multitude of factors involved, and the uncertainty concerning the true mechanisms, it is not surprising that reliable predictive tools of general validity are not available at present, even for flooding in fairly large diameter pipes. The most widely used correlation for the flooding limit in vertical tubes, although quite often unsuccessfully (Bankoff and Lee, 1986), is due to Wallis (1969):

$$\sqrt{U_G^*} + C_1\sqrt{U_L^*} = C_2 \tag{1}$$

where

$$U_G^* = U_G\sqrt{\frac{\rho_G}{gD(\rho_L - \rho_G)}} \tag{2}$$

$$U_L^* = U_L\sqrt{\frac{\rho_L}{gD(\rho_L - \rho_G)}} \tag{3}$$

with parameters $C_1 = 0.8$–1.0 and $C_2 = 0.7$–1.0, mainly depending on geometry. U_G and U_L are the gas and liquid superficial velocities respectively, ρ_G and ρ_L the phase densities, g the acceleration due to gravity and D the tube inside diameter. Many efforts have been made over the years (e.g. Bankoff and Lee, 1986) to improve the Wallis correlation by dealing with the coefficients C_1, C_2 and by introducing various dimensionless numbers to account for the observed effects of liquid properties. Typical of such efforts are the recent papers by Zapke and Kroeger (1996, 2000a,b), where data from relatively large tube diameters are employed.

In efforts to model flooding, quite often the characteristics of free falling films (in the absence of air flow) are invoked and utilized. A significant experimental observation (partly justifying this choice) is the fact (e.g. Nickling and Davidson, 1962; Zabaras and Dukler, 1988; Dukler et al., 1984) that the mean liquid film thickness (estimated by the Nusselt expression) remains essentially unaffected by the counter-current gas flow almost up to the critical flooding conditions. Therefore, it may be advantageous to use relevant information on wavy free falling films in order to clarify incipient flooding.

Wave evolution on free falling films has been reviewed by Chang (1994) from the stand point of wave dynamics, for the range of Reynolds numbers $O(10) < Re < O(10^3)$ which are of interest to this study. In this Re_L range long interfacial waves develop through amplification of infinitesimal disturbances introduced at liquid inlet. Reviewing experimental evidence, Chang classifies the wave evolution into four regions. Of particular interest here are regions III and IV; in region III "solitary waves" or "solitary humps" develop which are spatially distributed (on a flat surface) and of a "tear drop" shape. In the following region IV transverse variation and growth of those humps is observed so that adjacent crests may merge and pinch off. This type of clearly three-dimensional wavy flow (characterized by spatially distributed humps) has also been observed in this Laboratory (Vlachos et al., 2001) on a flat vertical surface. Furthermore, it is of particular interest that similar 3-D wave structures (strongly dependent on Re_L) have recently been recorded by Adomeit and Renz (2000) for film flow inside tubes of 46 and 54 mm i.d. It is not known, however, to what extent these coherent waves, resulting from gravity–capillarity induced instabilities (in the absence of gas/liquid interfacial shear), influence flooding phenomena.

Systematically obtained falling film data for flow *inside small i.d. tubes* are not available in the literature, to the authors' knowledge. Such data are presented here as part of the effort to clarify the influence of tube diameter on flooding phenomena.

In this paper a description of experimental equipment and procedures is presented first. Critical flooding velocities and related observations are given in a subsequent section. Experimental data on free falling films, obtained in the same test sections, are reported next. Various quantities are extracted from film thickness time records (e.g. film height, width, frequency spectra) to facilitate

interpretation of the flooding data, which is outlined in a subsequent section. In the Appendix A, appropriate expressions are developed for laminar free falling films in small i.d. tubes, different than the well-known Nusselt expressions strictly valid for flat surfaces.

2. Experimental set-up and procedures

An experimental flow loop (Fig. 1) was constructed to perform flooding experiments with various test section diameters (6–9 mm i.d.). The test tubes were made of glass and their inner diameter was measured using a laser-beam based method. Due to the sensitivity of flow regime transition to tube inclination, the test section has to be carefully adjusted. Air enters at the bottom, through a small tube (i.d. = 6 mm) placed concentrically, in a tapered entrance section designed to minimize disturbances and to promote development of air flow in contact with the falling liquid film. The latter is introduced uniformly at the top, through a specially machined porous wall segment, which is made of a ceramic material substituting a tubular section and fitted flash with the inner tube surface. An outer weir surrounds the porous wall section to facilitate a uniform liquid distribution. The liquid film develops along a straight tube of length 0.6 m. A bellmouth type liquid exit is provided to minimize end-effects. There is a small reservoir at the bottom of the bellmouth section where a constant liquid level is maintained that prevents air leakage. The two-phase mixture is separated using a cyclone located at the upper part of the test section. Air is released to

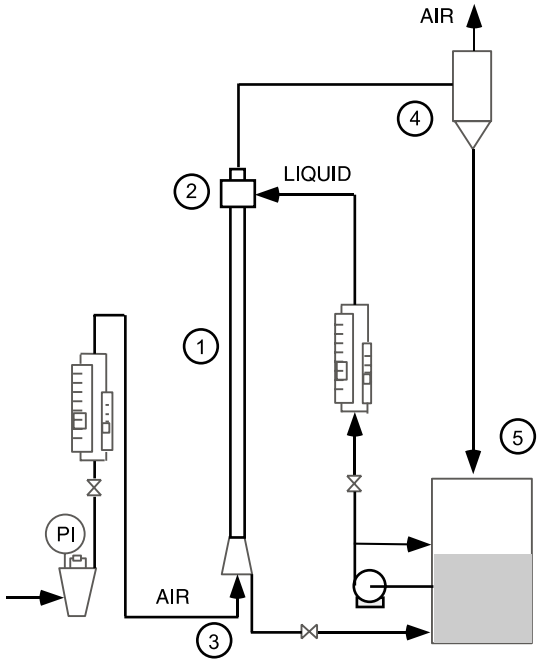

Fig. 1. Experimental flow loop: (1) test section; (2) porous wall segment; (3) tapered air-entrance section; (4) phase separator; (5) liquid storage tank.

Table 1
Physical properties

	Kerosene	Water
Density, ρ (kg/m^3)	800	1000
Viscosity, μ (kg/m s)	1.4e–03	1.0e–03
Surface tension, σ (kg/s^2)	0.028	0.072

the atmosphere while the liquid is collected in a small container and recirculated through the loop by means of a centrifugal pump.

Two liquids were used, namely water and kerosene, and their physical properties are presented in Table 1. In the case of water, it was necessary to improve the wettability of the glass tube inner surface by treating it before each set of experiments with a silica solution. The experiments were conducted at ambient temperature and pressure conditions. The pressure drop in the test section was measured using a differential pressure transducer.

Visualization experiments were carried out in order to investigate the flooding mechanism. Each flooding test started by first introducing the liquid; subsequently the air flow rate was progressively increased by small steps until reversal of the liquid flow was initiated. Initiation of liquid flow reversal, observed by naked eye and recorded, is described in detail in Section 3.2. The specific gas flow rate corresponding to the flooding point was also determined by monitoring the sharp increase of pressure drop.

Direct visual observations were made using a Redlake *Motion*Scope PCI® high-speed camera to capture the details of the basic mechanisms triggering flooding. The camera was fixed on a stand very close to the area of observation in such a way that the test section was located between the camera and the lighting system. The latter was comprised of several sources placed behind a diffuser to evenly distribute the light. The imaging system used was capable of recording up to 1000 full frames per second, but in the present experiments pictures were taken at a speed of 250 frames per second and a shutter rate of 1/1000 at three different locations along the pipe, i.e. just below the liquid entrance, at the liquid exit, and at an intermediate location.

One of the aims of the experimental work is to determine free falling film characteristics in the absence of gas flow. Consequently, the recorded images are used to extract *quantitative* information on the temporal variation of falling film thickness. With proper lighting the cross-section of the tube and the film are clearly outlined on the pictures as shown in Fig. 2. Using appropriate software the film trace can be obtained at a specific point along the tube. The calibration of the measuring system is accomplished by determining both the inner, i.d., and outer, o.d., diameter of the tube (Fig. 2), which are independently measured. It is pointed out here that the refractive index of the liquids employed and of the glass is rather close, and quite different than that of air. Therefore, with the optical system used, only two interfaces can be discerned; i.e. the (fixed) outer air/tube interface and the (varying) inner liquid/air one. This is shown in Fig. 2 where one can recognize the tube i.d. and o.d., the dry tube thickness, t, as well as the image of a falling film, superposed on the tube wall thickness and identified by a "total thickness", H. The actual liquid film thickness is obtained by subtracting the known wall thickness, t, from the measured "total thickness", H. This procedure is used to determine liquid film thickness at various locations in the test section.

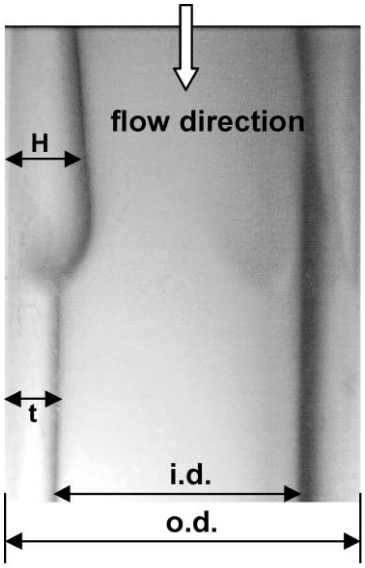

Fig. 2. A picture captured at liquid flow initiation (i.d./o.d.) inside/outside tube diameter, (t) dry tube thickness and (H) total thickness.

Pierson and Whitaker (1977) argue that for falling liquid films a good estimate of the entrance length, L_e, required to reach a fully developed condition may be obtained by $L_e \approx h_\infty Re$. In the present experiments with kerosene, the entrance length for fully developed film flow is estimated (using the above relation) to vary between 2 and 35 cm. The film thickness measurements reported here are taken at $L \approx 2$ cm from top (i.e. just below liquid entry) and at $L \approx 60$ cm (i.e. above the liquid exit), the latter location considered sufficient to obtain a well-developed wave structure. To calculate statistical parameters of the film, a 500-point sample is employed, obtained over a period of 2 s with a 250 Hz sampling frequency.

3. Flooding in small diameter tubes

3.1. Critical flooding velocities

In this section an overview is provided of critical flooding velocities, determined by means of visual observations and fast recordings, in tube diameters 6–9 mm. Each data point represents incipient flooding conditions as defined in Section 1 and generally accepted in the literature (Bankoff and Lee, 1986). An account of detailed visual observations and description of flow patterns is provided in the next section.

In Fig. 3(a)–(d) the data are plotted in terms of superficial gas velocity, at incipient flooding, versus the corresponding liquid Reynolds number $Re_L = 4\Gamma/v$. The superficial gas velocity corresponds to inlet conditions and due to the small pressure drop it does not significantly change along the tube. Three distinct regions can be readily observed (marked in Fig. 3a).

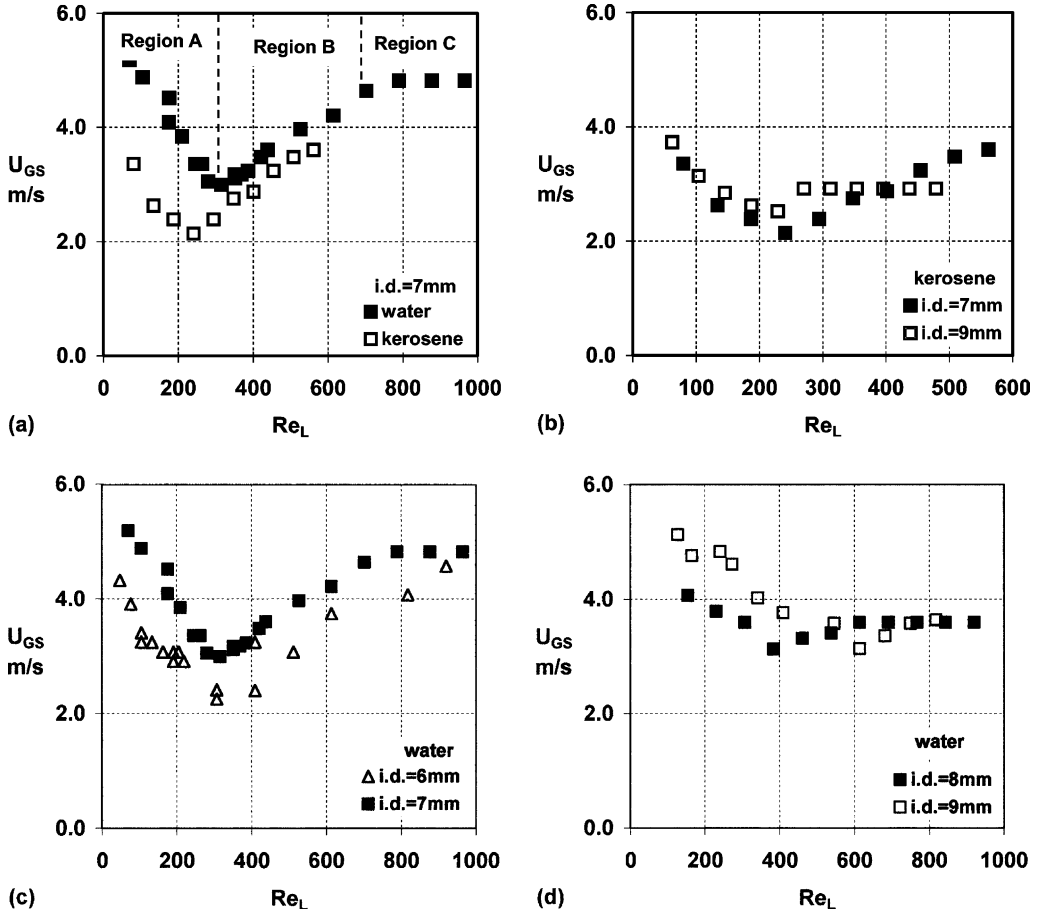

Fig. 3. Critical gas flooding velocities versus liquid Reynolds number. (a) Typical regions in a small i.d. (7 mm) tube; (b) data for kerosene; (c) data for water in 6 and 7 mm i.d. tubes; (d) data for water in 8 and 9 mm tubes.

In *Region A*, which corresponds to low Re_L, the flooding velocity is nearly *inversely proportional* to Re_L as one would have expected on the basis of previously published studies. This region extends up to a transition Reynolds number, Re_t, which depends on the liquid properties; e.g. $Re_t = 250$ for kerosene and $Re_t = 300$ for water in a 7 mm i.d. tube (Fig. 3a). This region can be clearly identified in all the data sets. Moreover, these data exhibit general trends reported in the literature for larger diameter tubes; i.e. decreasing flooding velocities with decreasing tube i.d. and decreasing surface tension.

Region B. For smaller i.d. tubes (Fig. 3a and c) there is an intermediate region, that is for $Re_L > Re_t$, where the flooding velocity tends to be *proportional* to Re_L. The extent of this region is reduced as the tube diameter increases and tends to disappear for the larger tube diameters (i.e. 9 mm). To the authors best knowledge the existence of this region has not been reported in the literature where most of the data have been obtained with much larger diameter tubes. However, it must be pointed out that in the data of Imura et al. (1977) (Fig. 3 of their paper) for flooding in

a 11.2 mm tube one can identify a similar region, but the authors pay no attention to it and offer no comments on this behavior.

Finally, in all the data sets, there appears to be another transition, i.e. a Reynolds number above which the flooding velocity tends to be constant and independent of the liquid flow rate (*Region C*). This constant flooding gas velocity exhibits a rather strong dependence on tube *diameter*, and (quite unexpectedly) it is generally greater for the smaller diameter tubes as shown in Fig. 3b–d.

3.2. Visual observations on flooding

At relatively small Reynolds numbers (Region A) the laminar liquid film is thin and a counter-current annular flow is clearly established prior to flooding. The film surface near the liquid entrance appears to be smooth and undisturbed, while coherent waves develop further downstream (Fig. 4a), that seem to cover the entire circumference as they travel towards the exit (Fig. 4b). The wave shown in Fig. 4a appears to be similar to those recorded by Adomeit and Renz (2000) at Re_L below 280 and to "humps" described by Chang (1994) for free falling films. In general, the interface characteristics before flooding are similar to those observed in laminar free falling films without counter-current air flow as will be discussed in a subsequent section.

The recordings clearly show that in Region A the flow reversal is initiated *at the liquid exit*, where an increase of the gas velocity results in the "levitation" of waves momentarily followed by the reversal of the liquid flow direction. The observed sequence of events suggests that the drag forces exerted by the gas flow on the wave become large enough to carry it upwards, overcoming gravitational forces. These observations are in agreement with recent literature results and in particular with the calculations of Jayanti et al. (1996) for vertical counter-current flow.

The upward motion of the liquid is characterized by periodicity; namely, after a mass of liquid has been transported upwards past the entry section, total liquid flow downwards is restored until a new wave is arrested near the exit, and the process is repeated. During the period of observations the gas flow rate is kept constant.

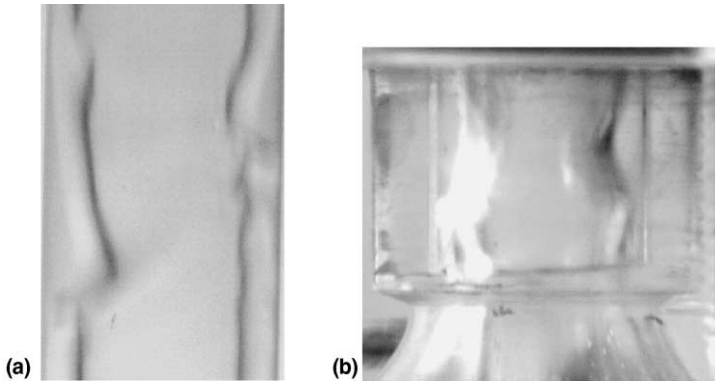

Fig. 4. Wave formation just before flooding (~50 ms) for kerosene in Region A: $Re_L = 62$; i.d. = 9 mm. (a) Formation of coherent waves far from the liquid entrance and (b) a wave arrested at liquid exit.

In Region B flooding also occurs by the *upward transport of waves* from near the bottom of the test section, in a manner similar to that observed for Region A. However, in this case the required gas velocity for incipient flooding tends to increase with increasing liquid flow rate, as shown in Fig. 3. At first look, the recordings do not display any drastic changes of the liquid layer that might account for this unexpected tendency. The only relevant observation made (requiring additional experimental support) is that, in Region B, with increasing Re_L there is no noticeable increase of liquid wave amplitude in the tube. After flooding is established, it is observed that cocurrent flow above the liquid inlet zone may coexist with some counter-current flow below inlet, i.e. there is partial liquid downflow. This low liquid flow rate is still capable of producing *secondary flooding*.

At relatively high liquid input (Region C) the recordings show that, for the smallest diameter tubes tested (i.e. i.d. = 6 and 7 mm), flooding is initiated at the liquid *inlet*. Fig. 5a includes a sequence of pictures showing incipient flooding just below the liquid inlet, where a local disturbance wave tends to grow and block the tube, leading to flow reversal. Moreover, a rather small portion of the liquid continues to move downwards and this flow causes a secondary flooding (Fig. 5b) at some point along the tube through a mechanism similar to that holding for Region A. On the contrary, in the larger diameter tubes (i.e. for 8 and 9 mm i.d.) flooding is initiated near the liquid *exit* and appears to be caused by wave growth. As the air flowrate increases, larger

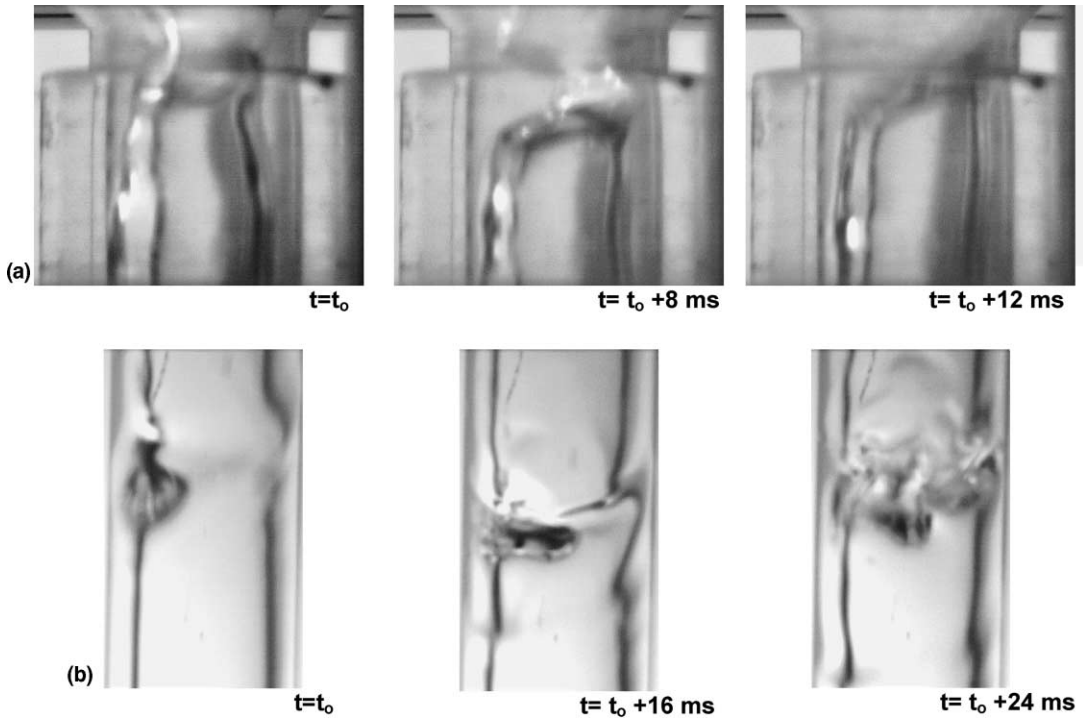

Fig. 5. (a) Incipient flooding at liquid entrance; (b) secondary flooding at a point along the pipe (Region C, kerosene/air, $Re_L = 500$, i.d. = 7 mm).

amplitude waves are formed (and occasionally droplets are torn off their crests); these waves reach a critical size and are swept upwards by the gas flow.

It should be pointed out that, in the range of liquid input rates of the present tests, total occlusion of the tube cross-section by liquid was not observed by naked eye or detected in the fast recordings.

4. Free falling film characteristics

Kerosene was used for measurements and observations of free falling film characteristics, since its lower surface tension promotes the formation of relatively larger amplitude (well-formed) waves and thus facilitates the recording of better quality images of the liquid film fluctuations by the optical method used. Typical traces of the measured film thickness are presented in Fig. 6 corresponding to the tube bottom (near the liquid exit), for $Re_L = 80$ and 350. The increase of both the mean film thickness and the amplitude of film thickness fluctuations with Re_L is evident. Furthermore, one may recognize *the substrate*, that is a region of small thickness in-between the large waves. The front of the large waves, usually starting from the substrate, has a greater slope than their back as expected. The time series of the film thickness data are statistically analyzed to obtain the main film characteristics, namely the mean film thickness, h, the root mean square of

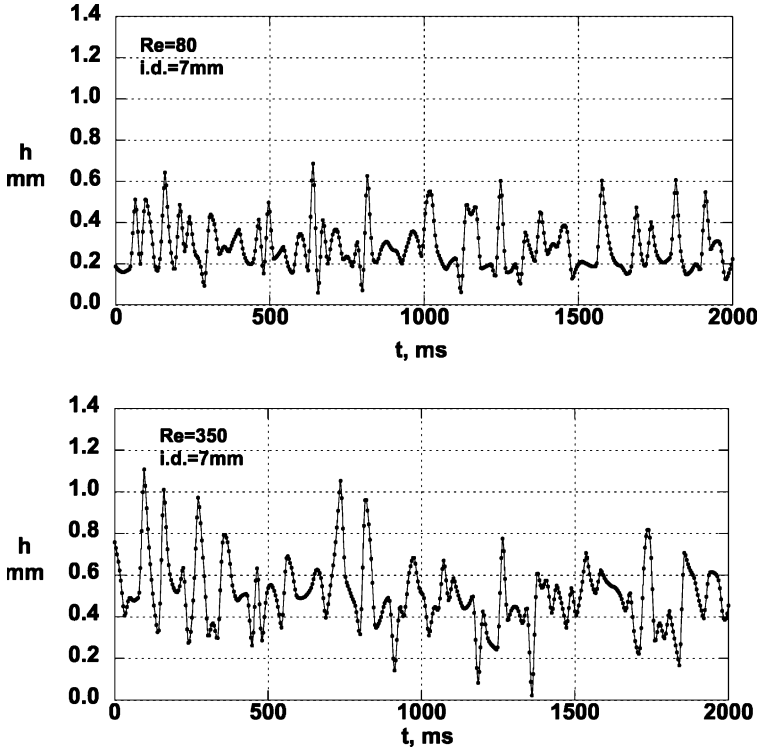

Fig. 6. Free falling film traces near the liquid exit for two Reynolds numbers ($Re_L = 80$ and 350).

Table 2
Free falling film characteristics of kerosene at two positions along the pipe

i.d. (mm)	Position	*Re*	h_{Nu} (mm)	h_0 (mm)	h (mm)	h_{rms} (mm)	h_w (mm)	h_s (mm)	Δh (mm)
7	Top	80	0.27	0.27	0.19	0.02	0.46	0.16	0.30
	Bottom				0.29	0.11			
	Top	240	0.38	0.40	0.29	0.03	0.60	0.10	0.50
	Bottom				0.37	0.14			
	Top	350	0.43	0.45	0.39	0.02	0.75	0.23	0.52
	Bottom				0.51	0.16			
9	Top	62	0.24	0.24	0.26	0.04	0.43	0.11	0.32
	Bottom				0.25	0.14			
	Top	187	0.35	0.36	0.17	0.10	0.75	0.19	0.56
	Bottom				0.45	0.22			
	Top	270	0.40	0.41	0.25	0.12	0.81	0.17	0.64
	Bottom				0.50	0.24			
	Top	395	0.45	0.47	0.32	0.03	0.78	0.20	0.58
	Bottom				0.46	0.21			
	Bottom	480	0.48	0.50	0.54	0.16	0.85	0.25	0.60

the film thickness, h_{rms}, the maximum wave height, h_W, and the substrate thickness, h_s (both with respect to the solid wall) as well as the height above the substrate $\Delta h = h_W - h_S$. Values of these film characteristics obtained from the data are summarized in Table 2. The film thickness, h_0, corresponding to a fully developed laminar free falling film, flowing *inside small diameter tubes*, is obtained from the following expression (briefly discussed in the Appendix A):

$$Q = \frac{\pi \rho g R^4}{8\mu}[(1-\lambda^2)(1-3\lambda^2) - 4\lambda^4 \ln \lambda] \quad \text{where } \lambda = \frac{R-h_0}{R} \tag{4}$$

and is included in Table 2 for comparison. The value of h_0 obtained from Eq. (4) is more representative of the problem treated here than the well-known Nusselt mean film thickness, h_{Nu}, which corresponds to flow on a flat surface and is, therefore, independent of tube diameter. It must be noted that the tabulated values of maximum wave height (i.e. the average value of wave peak height, h_W), extracted from cumulative distributions, correspond to a film thickness with probability of occurrence 95%, whereas those of the substrate height, h_S, correspond to a film thickness with probability of occurrence 5%.

Fig. 7 presents the variation of mean film thickness with liquid Reynolds number for 7 and 9 mm i.d. tubes. There is fair agreement of experimentally determined values of mean film thickness with the theoretical ones for smooth laminar films, predicted by means of Eq. (4). The deviation of a few data points, at intermediate Re_L, by 10–20% may be attributed to experimental error.

In Fig. 8 the mean substrate thickness, h_s, and the mean wave height, h_W, are plotted against the corresponding film Reynolds number. It appears that the mean substrate thickness remains nearly constant over a broad range of liquid flow rates, whereas the mean wave height exhibits a rather strong dependence on Reynolds number at small Re_L and tends to an asymptotic value above $Re_L = 250$. The influence of these falling film characteristics on flooding phenomena is discussed in a subsequent section.

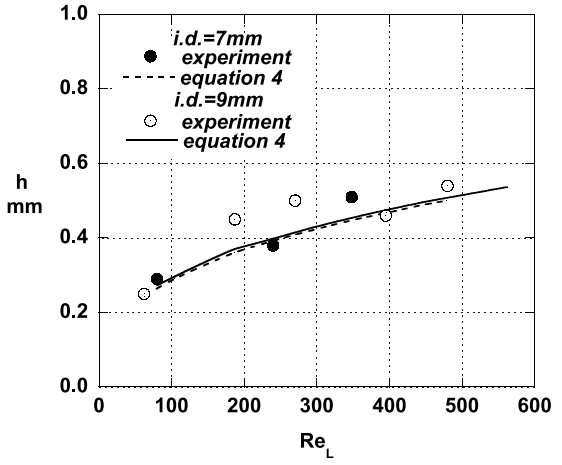

Fig. 7. Mean free falling film thickness versus liquid Reynolds number: comparison of experimentally determined thickness with prediction based on Eq. (4).

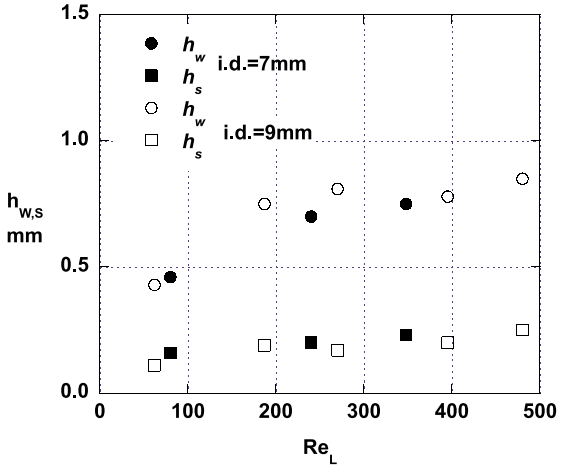

Fig. 8. Free falling film characteristics (kerosene, developed flow), (h_w) mean wave peak height; (h_s) substrate thickness.

The *intensity* of film thickness fluctuations is defined as h_{rms}/h, where h and h_{rms} are the local values of the time average film thickness and its standard deviation, respectively. Fig. 9 shows that the highest values of intensity are observed at low liquid flow rates. It is also interesting that the intensity is considerably smaller for the smallest tube i.d., which may have a bearing on the unexpected trends in the critical flooding velocity.

The wave height above the substrate, Δh, is plotted versus the corresponding film *Re* in Fig. 10. It appears that this quantity attains asymptotically a maximum value in the neighborhood of $Re_L = 300$ for both tube diameters. Δh may be related to h_{rms} through:

$$\Delta h = 2\sqrt{2}(h_{rms}) \tag{5}$$

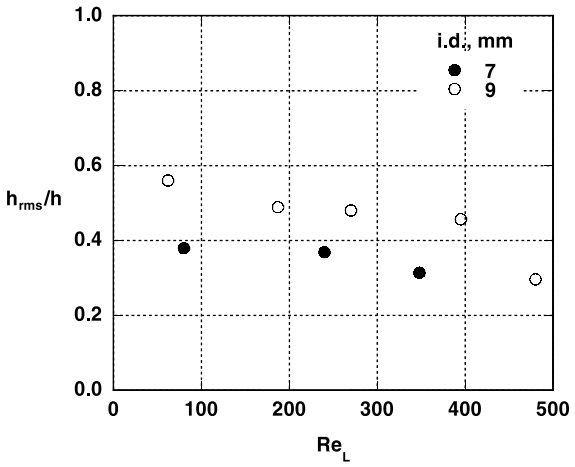

Fig. 9. Intensity of film thickness fluctuations versus the corresponding liquid Reynolds number, in free falling films.

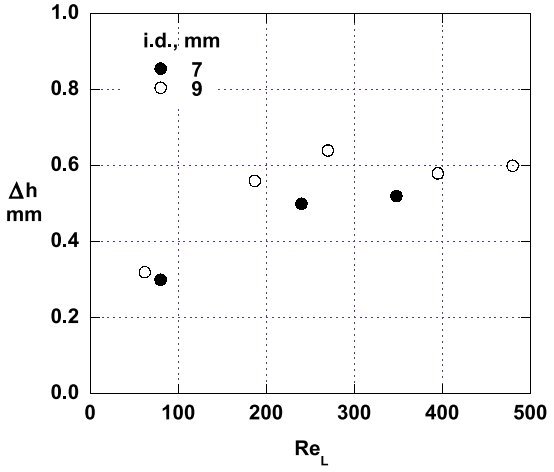

Fig. 10. Wave height above substrate versus the liquid Reynolds number for tube i.d. 7 and 9 mm, in free falling films.

for the ideal case of sinusoidal waves of amplitude $\Delta h/2$. It is interesting that the present data display a similar correlation.

The power spectral density (PSD) of the film height time series have been obtained by averaging modified periodograms, as reported by Paras and Karabelas (1991). Typical spectra are presented in Fig. 11 and display a very pronounced maximum, at frequencies between 7 and 13 Hz for all Re_L. There is also evidence from the fast camera recordings that this dominant frequency corresponds to the large waves on the film surface.

In view of the above results, it is interesting to inspect some instances of wave evolution, captured by the fast camera, such as those of Figs. 12 and 13. The former (Fig. 12) depicts the wavy film surface in the 9 mm i.d. tube for three Re_L corresponding to flooding regions A, B and C.

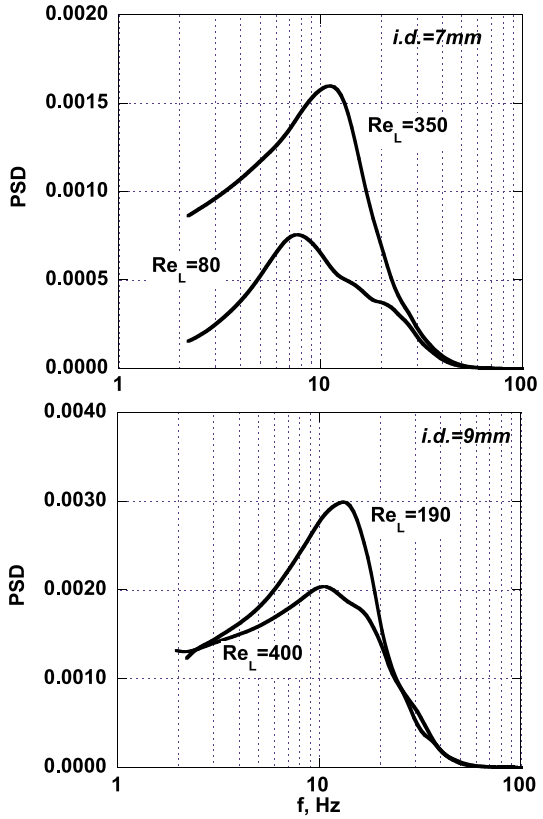

Fig. 11. PSD of the film height, in free falling films.

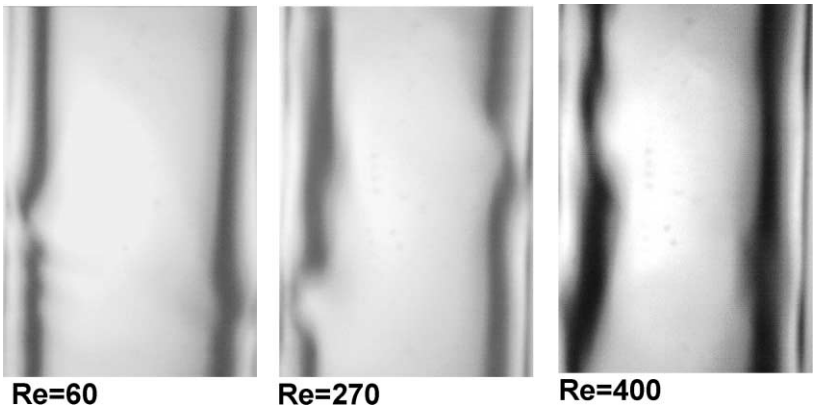

Fig. 12. Free falling film surface in the 9 mm i.d. pipe for three Re_L.

In all three cases, quite *coherent* waves appear to move downwards with no significant qualitative differences. Similar pictures are obtained at relatively small Re_L with the smaller tube i.d. (e.g. 7 mm). However, in the latter case, with increasing Re_L, the waves appear to be *less coherent* and

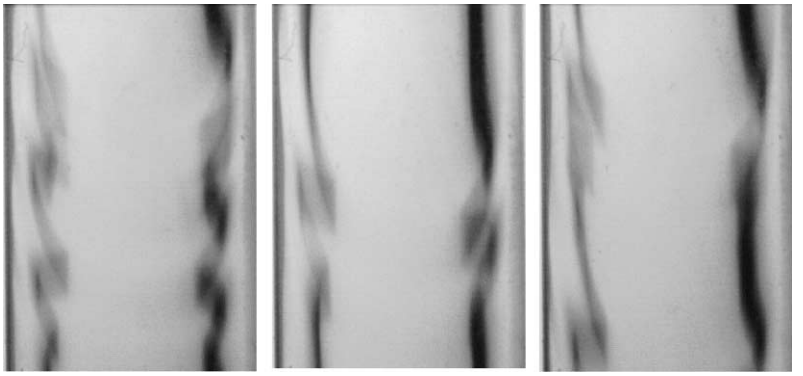

Fig. 13. Wave forms of free falling film (in the 7 mm tube at high Reynolds numbers, $Re_L = 500$) near the tube bottom.

more chaotic (as shown in Fig. 13), possibly due to some kind of wave interaction. It may be argued here that the greater tube curvature (for smaller i.d.) significantly influences wave evolution, by hindering the unrestricted lateral growth of waves and by promoting wave interactions. It is, therefore, likely that such small diameter effects on falling film characteristics will play a significant role on flooding phenomena.

5. Discussion of results

The above free falling film characteristics are helpful in elucidating the flooding mechanisms in the small diameter tubes tested.

In Region A coherent waves grow on the falling film moving towards the liquid exit. The motion of one of these large waves may be "arrested" by the counter-current gas flow leading to its rapid growth until the drag force exerted by the gas is large enough to overcome the gravity force and transport it upwards. This mechanism has already been described by several researchers (e.g. Hewitt, 1995). Furthermore, one may employ a Wallis type expression (Eq. (1)) with $C_2 = 1$ for data correlation as shown in Fig. 14; in the latter, the new data for Region A are included. According to Hewitt (1995) the value of parameter C_2 is in the range 0.7–1.0, where the lower values correspond to tubes with "sharp" end conditions and the upper values for tubes with porous wall and bellmouth ends, as in the present case. The data by Koizumi and Ueda (1996) from relatively small diameter tubes (i.d. = 10–26 mm) also correspond to Region A of the present experiments ($(U_L^*)^{0.5} < 0.5$) and may be correlated by a Wallis type equation. The value of constant C_2 corresponding to their data is smaller than 1.0 due to the gas injection method, which promotes flooding.

No and Jeong (1996) considered the roll wave instability as a possible flooding mechanism and developed a flooding model by studying hyperbolicity breaking near a singular point. The validity of this model is tested against data from Region A in Fig. 15. The parameters necessary for the model are the average wavelength before flooding, λ_w, and the liquid fraction, a_f, at the crest of the wave. The average wavelength, λ_w, is obtained from the video recordings, whereas the liquid

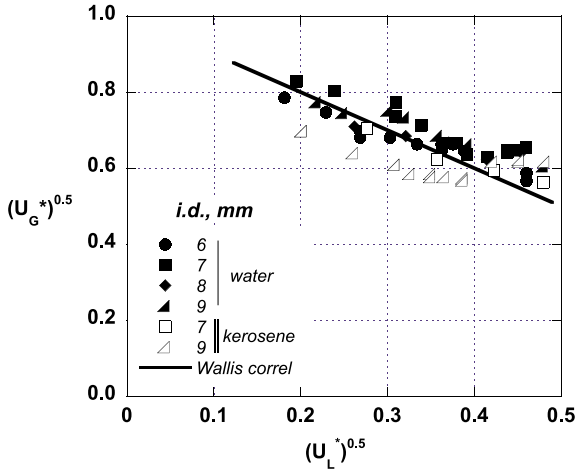

Fig. 14. Comparison of experimental data with the Wallis correlation of the form: $\sqrt{U_{\mathrm{L}}^*} + \sqrt{U_{\mathrm{G}}^*} = 1$.

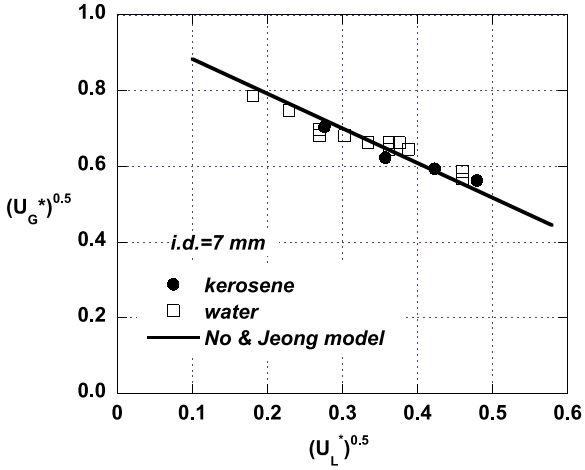

Fig. 15. Comparison of experimental data with the model proposed by No and Jeong (1996).

fraction, a_{f}, is estimated using the method proposed in their paper. The comparison of the present data with this model shows good agreement.

The free falling film characteristics tend to support a simple physical interpretation of flooding in Region A, which is based on the drag force exerted by the gas on the waves. The magnitude of this force depends on the wave shape, i.e. the wave height and in particular the height above the substrate, Δh. The falling film data of the present study show that, for relatively small Reynolds numbers (corresponding to Region A), Δh tends to increase with increasing Re_{L}; consequently, the gas velocity required to initiate the reversal of the wavy flow should decrease, as observed.

The tendency of flooding data in Region B, where the critical gas velocity is nearly *proportional* to liquid flow rate, is more difficult to explain. Considering that gravity plays a dominant role, one

can resort to falling film characteristics to interpret the flooding data. Above a transition Re_L (250, for kerosene and 7 mm i.d. tube) it is observed that the wave height (h_w) and the height above the substrate (Δh) tend to remain roughly constant (Figs. 8 and 10). Moreover, the dominant wave frequency in this Re_L range does not seem to change significantly (Fig. 11). These film characteristics suggest that, with increasing Re_L in Region B, both the wave celerity and the mass conveyed by a wave will tend to increase. Therefore, it is reasonable to expect an increase (with Re_L) of the gas velocity required to counterbalance the increasing gravitational and inertial forces, leading to liquid flow reversal.

A key question to be answered here is why above a transition Re_L (250–300) the wave height is rather insensitive to an increasing liquid flow rate. Damping of waves is a plausible answer. From previous studies (Chang, 1994; Adomeit and Renz, 2000) one may recall that in this Re_L-range U-shaped waves dominate. In the small i.d. tubes the growth of such waves in the lateral direction cannot be accommodated, possibly leading to interaction of wave tails (sides) and to damping. These effects seem to be more pronounced in the smaller i.d. used (6 and 7 mm) as one might have expected. It is noted that visual observations (e.g. Fig. 13) tend, in general, to support this explanation. There are no experimental data in the literature with a trend similar to that of Region B, because it is apparently observable only in small diameter tubes (i.e. for i.d. below $\approx$10 mm). However, this trend can be detected in the data of Imura et al. (1977) in a 11.2 mm pipe.

In Region C, which corresponds to the highest liquid flow rates employed, the air flooding velocity is nearly constant (i.e. independent of the liquid flow rate). Depending on the tube diameter, two different mechanisms are observed to be responsible for the onset of flooding. In the 8 and 9 mm tubes for both liquids tested, a finite amplitude wave formed close to the liquid exit rapidly grows and *chokes* the flow. The liquid is then pushed up as a liquid *slug* or as a mixed *entrained* phase. This type of flow has also been observed by other investigators (Moalem Maron and Dukler, 1984; Imura et al., 1977).

A different mechanism prevails in tube i.d. $\leqslant 7$ mm, where the falling film pictures reveal that the waves are not coherent (Fig. 13). An explanation similar to that, advanced for Region B (wave damping), may also be applicable here. In this case flooding occurs due to blockage just below the liquid entrance (Fig. 5), but at fairly high gas velocities. It is speculated that the cause of *entrance* flooding at these high liquid rates is the thickening of the liquid film at the entrance porous section. At the same time a rather small portion of the liquid flow continues to move downwards and may be responsible for the occurrence of a "secondary flooding" near the liquid exit, as already described for Region B.

The data clearly show smaller flooding velocities for the lower surface tension kerosene compared to those of water. As one would have expected, small surface tension is associated with increased wave instability and growth that promote flooding. To take into account the effect of fluid properties and conduit dimensions a correlation is presented by using gas/liquid Froude numbers and the Bond number. In Fig. 16a and b the data are plotted in terms of gas Froude number based on superficial gas velocity, at incipient flooding, versus the ratio of the corresponding liquid Froude number over the Bond number, where the Froude and Bond numbers are defined as:

$$Fr_{L,G} = U_{L,G}^2 \rho_{L,G} / gD(\rho_L - \rho_G) \tag{6}$$

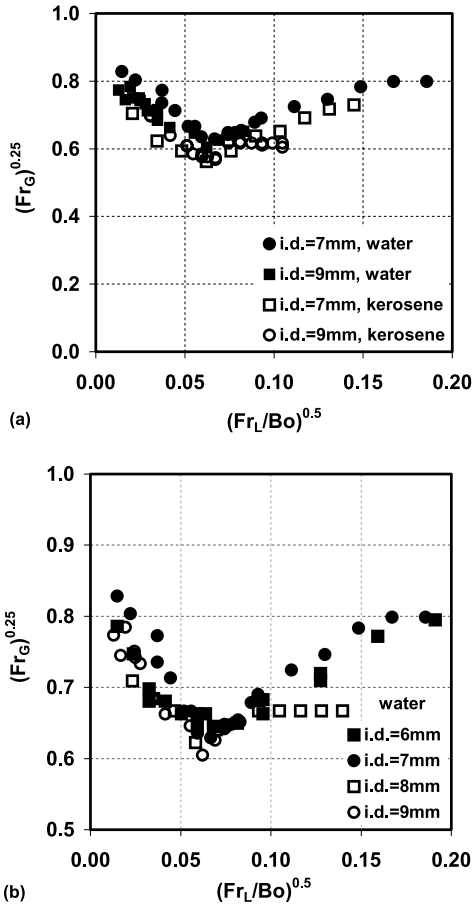

Fig. 16. Critical gas Froude number versus the ratio of liquid Froude to Bond number. Typical curves for (a) water and kerosene; (b) water.

$$Bo = D^2 g(\rho_L - \rho_G)/\sigma \tag{7}$$

The data are brought together reasonably well. It is noteworthy that the transition from Region A to B takes place at a constant value of the quantity $(Fr_L/Bo)^{0.5} = 0.06$ regardless of type of liquid and tube size employed in this study.

6. Concluding Remarks

The measured parameters of the falling film (mean thickness, wave height, substrate thickness etc.) suggest that the small tube i.d. plays a significant role in wave evolution and film development. It appears that wave growth is hindered in the small i.d. tube, possibly due to interaction of the tails of skewed (U-shaped) traveling waves. The nearly constant wave height with increasing Re_L (above a certain transition Reynolds number Re_t) is indicative of damping of waves. It is

interesting that the transition, at $Re_L = 250$–300, is very near the value ($Re_L = 300$) quoted by Adomeit and Renz (2000) as the transition to surgelike waves and turbulence spots in the film, in their experimental set-up.

The falling film characteristics seem to essentially determine the flooding behavior of small diameter tubes. Indeed, the transition from Region A to Region B appears to be related to the aforementioned damping of waves which is associated with an increasing gas velocity (with increasing Re_L) required to cause liquid flow reversal and flooding. Such a trend is not observed in larger diameter tubes. These wave interactions and damping effects might also be the reason for observing higher flooding velocities in the smaller tube diameters (6 and 7 mm), compared to those for 8 and 9 mm i.d., for high Re_L (Region C).

In all cases (with one exception) throughout the range of Re_L tested here, flooding is initiated at the tube bottom (liquid exit). Only with the smallest i.d. tube (6 and 7 mm) at high Re_L (Region C) top flooding is observed.

The effect of liquid properties (i.e. viscosity, surface tension) on flooding is in the direction expected, with the small surface tension kerosene exhibiting more unstable waves and thus smaller critical flooding velocities.

Flooding velocities can be reasonably well correlated with a Wallis-type expression only at small Re_L (Region A). From the viewpoint of practical application of results, it may be significant that beyond Region A (i.e. at relatively high Re_L) the critical flooding velocity tends to increase; taking water in a 7 mm tube as an example, the critical flooding velocity for $Re_L = 500$ is the same as that for $Re_L = 180$. This trend is considered beneficial for operating compact condensers, as it may broaden their region of operability. An estimate of the transition Reynolds number (from Region A to B) for small i.d. tubes may be obtained from the expression $(Fr_L/Bo)^{0.5} \approx 0.06$, although more data are required to test its reliability.

In closing, it will be pointed out that additional work is needed to better understand film flow development and flooding phenomena in small i.d. tubes.

Acknowledgements

Financial support by the European Commission under contract JOE3-CT97-0062 is gratefully acknowledged.

Appendix A. Laminar free falling films inside small diameter tubes

This type of steady flow is described in cylindrical coordinates (r, z) by

$$\frac{d(r\tau_{rz})}{dr} = (\rho g)r \tag{A.1}$$

with boundary conditions

$$\tau_{rz} = 0 \quad \text{at } r = R - h_0$$
$$u_z = 0 \quad \text{at } r = R$$

The origin of the coordinates is placed at the centerline of tube with radius R. The solution of this equation leads to the following expression for the velocity distribution.

$$u_z = \frac{\rho g R^2}{4\mu}\left[1 - \left(\frac{r}{R}\right)^2 + 2\left(\frac{R-h_0}{R}\right)^2 \ln\left(\frac{r}{R}\right)\right] \tag{A.2}$$

Consequently, using $\lambda = (R - h_0)/R$, the maximum and average velocities are given as

$$u_z|_{\max} = \frac{\rho g R^2}{4\mu}[1 - \lambda^2 + 2\lambda^2 \ln \lambda] \tag{A.3}$$

$$\langle u_z \rangle = \frac{\rho g R^2}{8\mu}\left[1 - 3\lambda^2 - \frac{4\lambda^4 \ln \lambda}{1-\lambda^2}\right] \tag{A.4}$$

The liquid film thickness h_0 is obtained from

$$Q = \frac{\pi \rho g R^4}{8\mu}[(1-\lambda^2)(1-3\lambda^2) - 4\lambda^4 \ln \lambda] \tag{A.5}$$

for a known liquid volumetric flow rate Q.

In Eq. (A.5), the function in the brackets is monotonically increasing with decreasing λ. Therefore, for a constant flow rate Q, to a reduced tube radius R corresponds a reduced λ value, i.e. an increased film thickness h_0. This tube size effect, which becomes significant at small i.d., is not included in the well-known Nusselt expression, developed for film flow on flat surfaces.

References

Adomeit, P., Renz, U., 2000. Hydrodynamics of three-dimensional waves in laminar falling films. Int. J. Multiphase Flow 26, 1183–1208.

Bankoff, S.G., Lee, S.C., 1986. A critical review of the flooding literature. In: Hewitt, G.F., Delhaye, J.M., Zuber, N. (Eds.), Multiphase Science and Technology, vol. 2, Chapter 2. Hemisphere Corp., NY.

Cetinbudaklar, A.G., Jameson, G.J., 1969. The mechanism of flooding in vertical countercurrent two-phase flow. Chem. Eng. Sci. 24, 1669–1680.

Chang, H.C., 1994. Wave evolution on a falling film. Annu. Rev. Fluid Mech. 26, 103–136.

Clift, R., Pritchard, C.L., Nederman, R.M., 1966. The effect of viscosity on the flooding conditions in wetted wall columns. Chem. Eng. Sci. 21, 87–95.

Dukler, A.E., Smith, L., Chopra, A., 1984. Flooding and upward film flow in tubes-I Experimental studies. Int. J. Multiphase Flow 10, 585–597.

Hewitt, G.F., 1995. In search of two-phase flow, Lecture, 30th US National Heat Transfer Conference, Portland, Oregon.

Imura, H., Kusuda, H., Funatsu, S., 1977. Flooding velocity in a counter-current annular two-phase flow. Chem. Eng. Science 32, 79–87.

Jayanti, S., Tokarz, A., Hewitt, G.F., 1996. Theoretical investigation of the diameter effect on flooding in counter-current flow. Int. J. Multiphase Flow 22, 307–324.

Koizumi, Y., Ueda, T., 1996. Initiation conditions of liquid ascent of the counter current two-phase flow in vertical pipes (in the presence of two-phase mixture in the lower portion). Int. J. Multiphase Flow 22, 31–43.

Moalem Maron, D., Dukler, A.E., 1984. Flooding and upward film flow in vertical tubes-II Speculations on film flow mechanisms. Int. J. Multiphase Flow 10, 599–621.

Nickling, D.J., Davidson, J.F., 1962. The onset of instability in two phase slug flow. Proc. I. Mech. Symp. Two-Phase Flow, London, February, paper7.

No, H.C., Jeong, J.H., 1996. Flooding correlation based on the concept of hyperbolicity breaking in a vertical annular flow. Nucl. Eng. Des. 166, 249–258.

Paras, S.V., Karabelas, A.J., 1991. Properties of the liquid layer in horizontal annular flow. Int. J. Multiphase Flow 17, 39–454.

Pierson, F.W., Whitaker, S., 1977. Some theoretical and experimental observations of the wave structure of falling liquid films. Ind. Eng. Chem. Fundam. 16, 401–408.

Shearer, C.J., Davidson, J.F., 1965. The investigation of a standing wave due to gas blowing upwards over a liquid film; its relation to flooding in wetted-wall columns. J. Fluid Mech. 22, 321–335.

Wallis, G.B., 1969. One-dimensional two-phase flow. McGraw-Hill, New York.

Vlachos, N.A., Paras, S.V., Mouza, A.A., Karabelas, A.J., 2001. Visual observations of flooding in narrow rectangular channels. Int. J. Multiphase Flow 27, 1415–1430.

Zabaras, G.J., Dukler, A.E., 1988. Countercurrent gas-liquid annular flow, including the flooding state. AICHE J. 34, 389–396.

Zapke, A., Kroeger, D.G., 1996. The influence of fluid properties and inlet geometry on flooding in vertical and inclined tubes. Int. J. Multiphase Flow 22, 461–472.

Zapke, A., Kroeger, D.G., 2000a. Counter-current gas–liquid flow in inclined and vertical ducts—I: Flow patterns, pressure drop characteristics and flooding. Int. J. Multiphase Flow 26, 1439–1455.

Zapke, A., Kroeger, D.G., 2000b. Counter-current gas–liquid flow in inclined and vertical ducts—II: The validity of the Froude–Ohnesorge number correlation for flooding. Int. J. Multiphase Flow 26, 1457–1468.